forests

MDPI

Article

Ecologically Constrained Multi-Task Deep Learning for Interpretable Joint Estimation of Mountain Forest Biomass and Growing Stock Volume

Jia Liu [1], Qingqing Huai [1], Yachao Li [2], Yunfei Yan [2], Peng Wang [2,*], Shuoshuo Liang [3], Yafei Shi [4] and Wendou Liu [5,*]

[1] College of Food Science and Engineering, Shandong Agriculture and Engineering University, Licheng District, Jinan 250100, China; liujia.alrc@gmail.com (J.L.); 18765868960@163.com (Q.H.)
[2] College of Forestry Engineering, Shandong Agriculture and Engineering University, Licheng District, Jinan 250100, China; liyczzy@163.com (Y.L.); lwyanyunfei@163.com (Y.Y.)
[3] School of Agriculture and Biology, Shanghai Jiao Tong University, No. 800 Dong Chuan Road, Shanghai 200240, China; liangshuoshuo0725@163.com
[4] College of Grassland Science, Gansu Agricultural University, Anning District, Lanzhou 730070, China; shiyafei2013@126.com
[5] Research Institute of Forestry Policy and Information, Chinese Academy of Forestry, Beijing 100091, China
* Correspondence: sdwp2010@163.com (P.W.); wdl_hubu@caf.ac.cn (W.L.)

Abstract

Reliable quantification of forest aboveground biomass (AGB) and growing stock volume (GSV) underpins carbon stock assessment and ecosystem monitoring. However, the complex mountainous terrain makes it difficult to estimate forest parameters, and research on the simultaneous estimation of forest AGB and GSV remains limited. To this end, this study proposed an eco-constrained explainable multi-task deep learning framework (Eco-AMT-MLP) that integrated Sentinel-2 data obtained from the Google Earth Engine platform with topographic, soil, and climatic factors to jointly estimate forest AGB and GSV while incorporating an ecological constraint linking the two prediction tasks in the complex mountainous forests of northwestern Yunnan Province. The model's performance was evaluated against Random Forest (RF), Extreme Gradient Boosting (XGBoost), Categorical Boosting (CatBoost), and K-Nearest Neighbor Regression (KNN), and ablation experiments were conducted to assess the contribution of the ecological constraint module. The Eco-AMT-MLP model demonstrated the best overall predictive performance among the compared models, achieving an R^2 of 0.64 ± 0.08 and an RMSE of 132.99 ± 19.96 m^3 ha^{-1} for GSV prediction, and an R^2 of 0.58 ± 0.07 and an RMSE of 87.37 ± 13.10 Mg ha^{-1} for AGB prediction. Compared with the MLP model, Eco-AMT-MLP increased the R^2 values for GSV and AGB predictions by 0.04 and 0.11, respectively, while reducing the corresponding RMSE values by 7.46 m^3 ha^{-1} and 10.12 Mg ha^{-1}, respectively. However, the model shows only limited improvement in AGB estimation accuracy, indicating that its enhancement of AGB estimation is less pronounced than its improvement of GSV estimation. SHAP analysis further identified environmental covariates and Sentinel-2 spectral features as important predictors of forest AGB and GSV. By integrating joint estimation of forest AGB and GSV with ecological constraints and interpretable predictor analysis, this framework provides a methodological reference for regional forest carbon-stock assessment, forest resource inventories, and ecosystem monitoring in complex mountainous regions.

Academic Editor: Choonsig Kim

Received: 21 September 2026
Revised: 29 October 2026
Accepted: 3 November 2026
Published: 4 November 2026

Copyright: © 2026 by the authors. Licensee MDPI, Basel, Switzerland. This article is an open access article distributed under the terms and conditions of the Creative Commons Attribution (CC BY) license.

Keywords: multi-source remote sensing; machine learning; multi-task deep learning; forest aboveground biomass; forest growing stock volume; Sentinel-2; ecological constraint; forest inventory

1. Introduction

Forest aboveground biomass (AGB) and growing stock volume (GSV) are key indicators of forest structure, productivity, and ecosystem condition [1]. AGB quantifies the mass of aboveground organic matter, whereas GSV describes the volume of standing woody material within a forest stand. Together, these metrics provide complementary information for assessing forest resources and ecosystem function. Conventional ground-based forest inventories, however, are costly, time-consuming, and spatially limited, which hinders rapid, large-scale assessment of forest attributes in complex mountainous terrain [2].

Remote sensing technology enables the rapid acquisition of forest resource data over large areas, providing a new approach to estimating forest AGB and GSV. Sentinel-2 optical data include visible, near-infrared, and red-edge bands, which can effectively capture the spectral response characteristics of the forest canopy and are widely used for estimating forest AGB [3]. Muhe et al. [4] estimated forest AGB using Sentinel-2 spectral bands, vegetation indices, and biophysical variables, demonstrating the effectiveness of Sentinel-2 data in remote sensing estimates of biomass ($r = 0.65–0.74$). In complex mountainous terrain, however, canopy spectra alone may not fully explain spatial variation in forest attributes, because elevation, slope, and aspect modify solar radiation, temperature, and water availability, while soil and climatic conditions influence nutrient supply and forest growth [5]. He et al. [6] pointed out that forest AGB is not only influenced by stand structure characteristics but is also closely related to topographic factors such as elevation and slope, indicating that environmental conditions play an important role in the spatial distribution of biomass. Integrating these topographic, soil, and climatic covariates with Sentinel-2 observations can therefore provide complementary ecological information for estimating forest AGB and GSV. The value of such multi-source integration is also evident in GSV estimation. A hierarchical model integrating UAV, Sentinel-2, and ground inventory data enabled regional-scale estimation of forest GSV [7]. Mura et al. [8] evaluated Sentinel-2 imagery for GSV prediction in two Italian forest areas, while Chrysafis et al. [9] found that texture features derived from Sentinel-2 improved GSV estimation compared with spectral features alone. Li et al. [10] further investigated feature selection, multispectral image fusion, and ensemble learning for GSV estimation. These studies demonstrate the potential of integrating multisource remote sensing data and advanced modeling methods for GSV estimation. However, the accuracy of GSV prediction may still be constrained by the limited structural information provided by optical imagery and variations in forest conditions, highlighting the need for more effective integration of remote sensing data and environmental information. In parallel, incorporating environmental covariates into Sentinel-2-based models improved AGB estimation [11]. Feature selection and ensemble learning enhanced GSV prediction from multi-source remote-sensing data [12]. Collectively, these studies support the use of integrated optical, environmental, and field observations for estimating both forest AGB and GSV in heterogeneous landscapes.

Beyond the choice of input variables, model design determines how effectively multi-source information can be used. Compared to traditional machine learning methods, deep learning models can automatically extract deep features from remote sensing and environmental data, thereby improving the ability to model complex nonlinear relationships [13]. Deep learning is not only applicable to single-parameter prediction but also enables joint learning across multiple related tasks through the sharing of network features [14].

By learning shared representations across tasks while retaining task-specific outputs, these models can jointly predict structural, biomass-related, and physiological traits, including leaf area, biomass, plant height, and chlorophyll content [15]. The TomPhenoNet multimodal multi-task network further integrates complementary data sources to predict multiple crop growth and yield traits, including plant height, leaf area, fresh weight, and fruit number [16]. Collectively, these studies demonstrate the feasibility of combining heterogeneous observations with shared and task-specific representations to exploit complementary information across prediction tasks and uncover common information among biologically related targets. However, the application of multi-task learning in forest remote sensing remains limited, particularly for the joint estimation of AGB and GSV.

However, the network architecture, loss function, learning rate, and other key parameters of deep learning models require careful optimization, making the training process difficult to adjust. Attention mechanisms can adaptively identify feature importance, reduce interference from redundant information, and enhance the fitting capabilities of deep learning models [17]. Previous studies have incorporated attention mechanisms into deep-learning models for AGB estimation, thereby enhancing the representation of multisource remote-sensing features [18]. In addition, an attention mechanism was integrated into the CNN–LSTM model for GSV estimation. This integration strengthened the representation of key remote-sensing features and improved the extraction of temporal information, resulting in enhanced predictive performance (R^2 = 0.84, RMSE = 26.73 $m^3 \cdot ha^{-1}$) [19]. Furthermore, as the core component of deep learning model optimization, the loss function directly influences the model's convergence process, generalization ability, and predictive performance [20]. In multi-task learning, discrepancies in task characteristics and optimization objectives may cause task conflicts, and improper loss weighting strategies may limit effective knowledge sharing across tasks. Yu et al. [21] demonstrated that gradient conflicts between different tasks can interfere with the optimization process in multi-task learning, potentially hindering effective knowledge transfer between tasks. In addition, balancing the losses associated with different tasks remains a key challenge, as inappropriate loss weighting may degrade model performance [22]. AGB and GSV both characterize the GSV of woody material at the stand level and are linked through structural and allometric relationships. However, the AGB–GSV relationship can vary with forest type, species composition, stand age, and management regime. Therefore, rather than imposing a universal fixed relationship, the AGB–GSV relationship characterized from field observations can be encoded as an ecological regularization term in the multi-task loss function. This term penalizes joint predictions that substantially deviate from the expected relationship. Such a constraint can establish a connection between the two tasks, thereby facilitating information exchange between them and coordinating the joint optimization process. In addition, building on these established AGB–GSV relationships and previous multi-task learning studies [23,24], this study uses the empirical relationship between AGB and GSV to establish an explicit association between the two prediction tasks. Rather than treating this relationship as a strict constraint, we incorporate it as a soft ecological constraint within a Sentinel-2-based, plot-level multi-task learning framework. In this way, the established ecological relationship provides additional cross-task information during model optimization while allowing AGB and GSV to retain their task-specific predictive characteristics.

This study focuses on the mountainous forests of northwestern Yunnan Province. By integrating Sentinel-2 remote sensing imagery with multi-source environmental factors, an ecological constraint attention-based multi-task MLP (Eco-AMT-MLP) was developed for the joint estimation of AGB and GSV. Unlike conventional multi-task models that primarily exploit shared representations across tasks, Eco-AMT-MLP combines attention-based feature representation with a soft ecological constraint derived from the empirical

relationship between AGB and GSV. This design not only enables joint learning of the two forest attributes but also incorporates their ecological relationship into the model training process. However, the potential of integrating the empirical relationship between AGB and GSV into a multi-task learning framework for their joint estimation has not been fully explored. To address this issue, Eco-AMT-MLP integrates this relationship as a soft ecological constraint, allowing ecological knowledge to inform the joint estimation of AGB and GSV. The objectives were to:

(1) Develop a multi-task deep learning framework that builds on the established empirical relationship between AGB and GSV by incorporating this relationship as a soft ecological constraint, and assess its applicability to Sentinel-2-based plot-level joint estimation of AGB and GSV in complex mountainous forests.

(2) Employ SHAP to quantify the contributions of individual features to AGB and GSV predictions and examine their associations with environmental conditions.

2. Materials and Methods

Figure 1 presents the overall framework for integrating multi-source data and jointly estimating aboveground biomass (AGB) and growing stock volume (GSV) in northwestern Yunnan Province. Sentinel-2 surface reflectance (SR) data and topographic, climatic, and soil variables were obtained through Google Earth Engine (GEE) and integrated with field inventory measurements to establish the dataset. Random Forest (RF) was applied for feature selection, followed by a performance comparison of several machine learning algorithms, including RF, KNN, XGBoost, and CatBoost. Subsequently, the Eco-AMT-MLP model was developed to jointly estimate AGB and GSV by incorporating feature attention and MLP (fully connected) network representations. In addition, the loss function was augmented with an ecological constraint to regulate model optimization, and SHAP was applied to reveal the contribution of each predictor to the predicted outcomes.

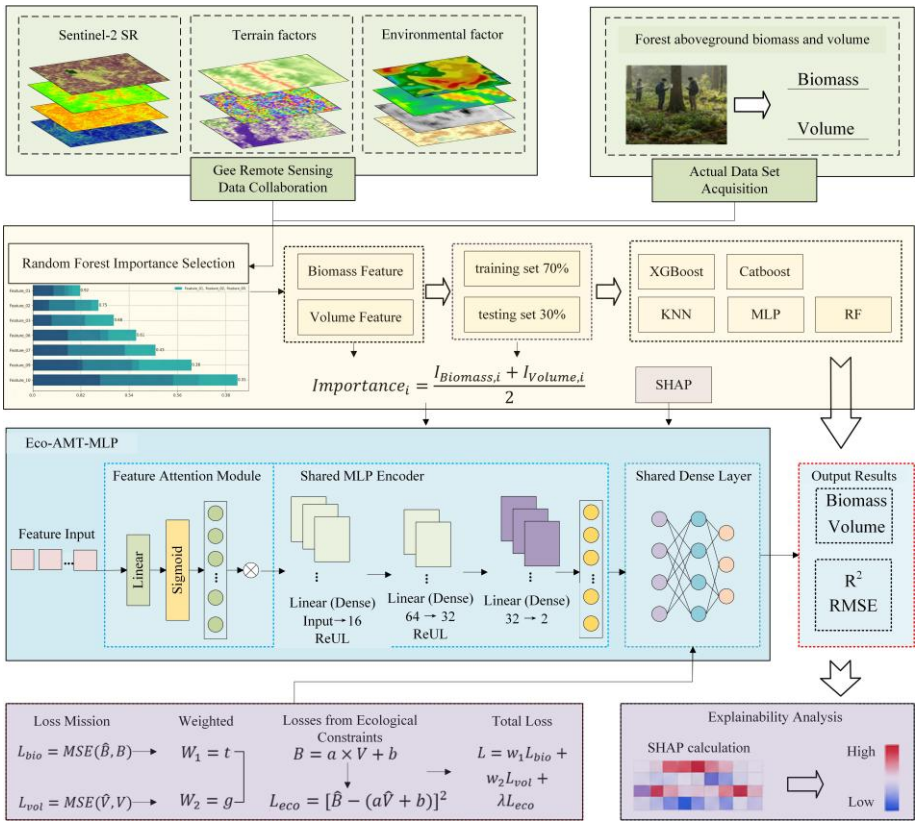


Figure 1. Research workflow diagram. Here, t and g represent the mean AGB and mean GSV across all plots, respectively, while the task weights are set to W_1 = 1 and W_2 = 1.4.

https://doi.org/10.3390/f17111318

2.1. Study Area

Northwestern Yunnan Province serves as the study region, comprising Lijiang City, Diqing Tibetan Autonomous Prefecture, and Nujiang Lisu Autonomous Prefecture. (25°00′–29°00′ N, 97°30′–101°30′ E), as shown in Figure 2. The region features complex mountainous terrain with significant variations in elevation (142 m–6145 m) [25]. Climatically, the study area is characterized by a low-latitude plateau monsoon climate, influenced by the southwest monsoon and complex topographic conditions. The mean monthly temperature of the warmest month (July) on the Yunnan Plateau is approximately 19–20 °C [26]. Annual precipitation ranges from approximately 400 to 4600 mm, with significant spatial variation [27]. The region supports diverse forest vegetation types, with dominant tree species including *Pinus yunnanensis* [28], *Pinus armandii* [28], *Pinus densata* [29], various *Quercus* species [30], and other evergreen broad-leaved tree species [31].

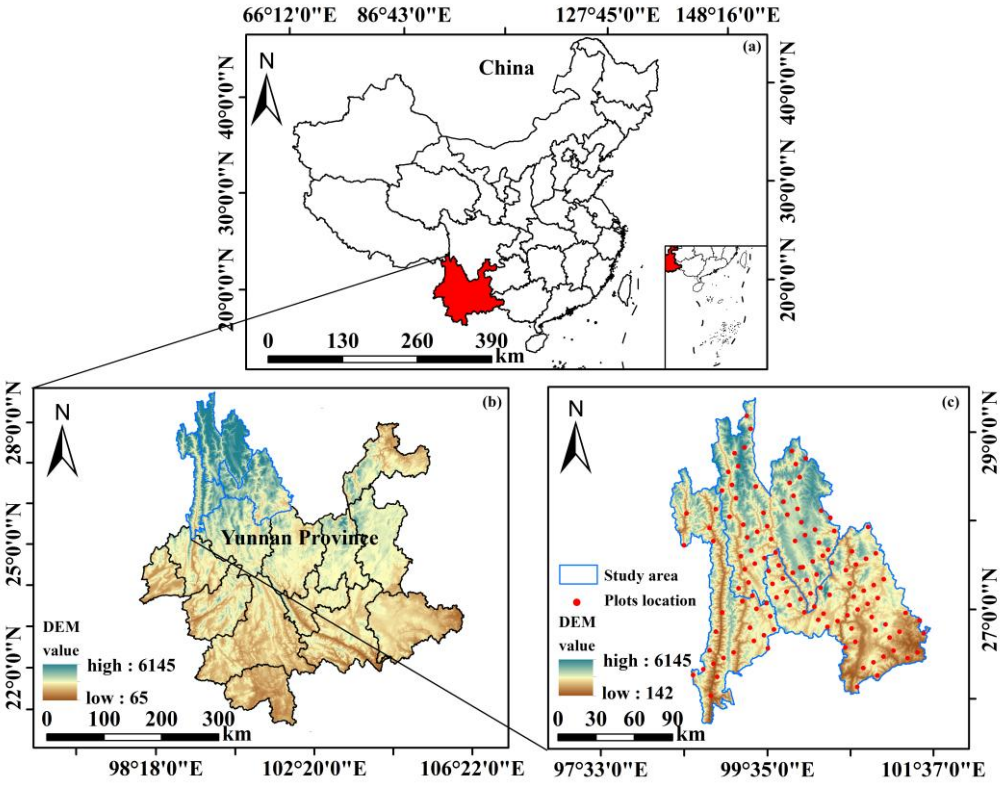


Figure 2. Location and extent of the study area: (**a**) Administrative divisions of China; (**b**) Administrative divisions of Yunnan Province; (**c**) The study area in northwestern Yunnan.

2.2. Data Collection and Estimation of Forest AGB and GSV

The forest inventory data used in this study were collected in 2021 in the northwestern part of Yunnan Province. A total of 127 sample plots were established, each measuring 30 m × 30 m. Kim et al. [32] compared the performance of 20 m × 20 m and 30 m × 30 m sample plots for estimating AGB, finding that the 30 m × 30 m plots yielded higher accuracy in both model fitting and validation. Field measurements were conducted in 2021 and matched to the Sentinel-2 annual median composite for the same year. The recorded stand characteristics included diameter at breast height (DBH at 1.3 m), tree height (H), forest type, stand age, and slope. DBH was measured for all trees with DBH ≥ 5 cm; Dg is the quadratic mean diameter, and H is the Lorey mean height, consistent with the tree-level equations used below. The distribution of the sample plots by forest type and stand age is also presented in Table A1. Descriptive statistics of the sample dataset are presented in Table 1. Because of the rugged terrain, high-elevation plots are difficult to access, and

the sample is therefore concentrated at lower, more accessible elevations, with the highest sampled plot at 4333 m [29]. Using DBH and H as tree-level measurement variables, corresponding tree AGB models and bivariate tree volume models were selected based on tree species. The parameters of the AGB models were determined according to the Technical Regulations for Tree Modeling (LY/T 2258–2014), and the parameters of the GSV models were determined according to the Technical Regulations for Inventory for Forest Management Planning and Design (GB/T 26424–2010) [33,34]. Plot values were aggregated to the 30 m × 30 m plot and matched to the Sentinel-2 pixel containing the plot centre. RTK positioning accuracy was within 0.03 m.

Table 1. Statistical parameters of the sample dataset.

Variables	Minimum	Mean	Maximum	SD
H (m)	2.7	11.60	32.0	5.92
Dg (cm)	6.8	18.9	68.3	10.89
AGB (Mg/ha)	7.89	147.61	593.49	128.35
GSV (m^3/ha)	9.53	209.51	1231.83	211.74

2.3. Collection of Remote Sensing Data and Variable Selection

2.3.1. Remote Sensing Data

In this study, Sentinel-2 imagery acquired in 2021 and environmental data including topography, climate, and soil were obtained for the study area using the GEE platform, with the Sentinel-2 imagery processed using annual median compositing. The Sentinel-2 imagery underwent preprocessing, including cloud removal and annual median compositing; 10 spectral bands were then extracted, and 9 vegetation indices were calculated from different band combinations [35]. Topographic data extract three features, including digital elevation models, slope, and aspect [36]. Environmental data primarily consist of 9 climate characteristics and 8 soil characteristics [11]. The 2021 China Land Cover Dataset (CLCD) was obtained from Zenodo (https://zenodo.org/records/5816591. accessed on 25 August 2026) and used to generate the forest mask by retaining areas classified as forest. All data were resampled to a consistent 30 m × 30 m spatial resolution, yielding 39 input variables that served as the basis for subsequent AGB and GSV estimation. Table 2 summarizes the remote sensing feature variables.

Table 2. Imagery sources and remote sensing variables.

Feature Type	Feature	Description	Calculation Formula
Sentinel-2	B2, B3, B4, B5, B6, B7, B8, B8a, B11, B12	Blue, Green, Red, Red Edge 1–3, NIR, Narrow NIR, SWIR 1–2	
Vegetation Index	CVI	Chlorophyll Vegetation Index	$CVI = \frac{B8 \times B4}{B3^2}$
	EVI	Enhanced Vegetation Index	$EVI = \frac{2.5 \times (B8 - B4)}{B8 + B4 \times 6 - 7.5 \times B2 + 1}$
	GCI	Green Chlorophyll Index	$GCI = B8/B3 - 1$
	MNDWI	Modified Normalized Difference Water Index	MNDWI = $(B3 - B11)/(B3 + B11)$
	MSI	Moisture Stress Index	MSI = $B11/B8$
	NDBI	Normalized Difference Built-up Index	NDBI = $(B11 - B8)/(B11 + B8)$
	NDRE	Normalized Difference Red Edge Index	NDRE = $(B8 - B5)/(B8 + B5)$
	NDVI	Normalized Difference Vegetation Index	NDVI = $(B8 - B4)/(B8 + B4)$
	NDWI	Normalized Difference Water Index	NDWI = $(B8 - B11)/(B8 + B11)$
	SAVI	Soil-Adjusted Vegetation Index	SAVI = $1.5\times \frac{B8-B4}{B8+B4+0.5}$

Topographic	DEM	Digital Elevation Model	-
	Slope	Slope	-
	Aspect	Aspect	-
Climatic Factor	pr	Precipitation	-
	tmmx	Maximum Temperature	-
	tmmn	Minimum Temperature	-
	pet	Potential Evapotranspiration	-
	aet	Actual Evapotranspiration	-
	soil	Soil Moisture	-
	vpd	Vapor Pressure Deficit	-
	srad	Solar Radiation	-
	def	Climate Water Deficit	-
Soil Factor	clay	Clay Content	-
	sand	Sand Content	-
	silt	Silt Content	-
	SOC	Soil Organic Carbon	-
	pH	Soil pH	-
	CEC	Cation Exchange Capacity	-
	BDOD	Bulk Density	-

2.3.2. Variable Selection

To reduce potential redundancy among candidate input variables, Random Forest (RF)-based feature selection was performed before model construction. The importance of each candidate variable for AGB and GSV estimation was assessed separately [37]. The importance rankings for both prediction targets were then jointly considered to select the top 10 shared input features [38], which were used for both AGB and GSV estimation. Of the 39 initial candidate variables, 10 were ultimately selected as model inputs.

2.4. Model Construction

2.4.1. Multi-Task Deep Learning Model Construction

The study developed a multi-task deep learning model (Eco-Attention Multi-Task Network, Eco-AMT-MLP) that integrates attention mechanisms and ecological relationship constraints to enable the simultaneous estimation of forest AGB and GSV. The model takes remotely sensed features that have undergone feature selection as input, uses an MLP (fully connected) network to extract feature representations relevant to the two prediction tasks, and sets up independent prediction branches for each task. Based on this, the ecological metric relationship between GSV and AGB is incorporated into the model's loss function as a soft penalty term, allowing ecological knowledge to guide the joint optimization of the two prediction tasks.

(1) Attention-Based Feature Extraction

The study introduces an attention mechanism to adaptively weight the input features. For an input feature vector X, feature weights are generated through a fully connected layer and the Sigmoid activation function:

$$W = \sigma(W_a X + b_a) \quad (1)$$

Here, W_a and b_a represent the weight matrix and bias term of the attention layer, respectively; $\sigma(\cdot)$ is the sigmoid activation function, and W denotes the attention weights corresponding to each input feature. The attention weights are then applied to the input features:

$$X_a = X \times W \quad (2)$$

Here, X_a represents the weighted feature representation. Through this mechanism, the model can automatically learn the relative importance of different features, enhance the contribution of key variables to the prediction results, and reduce the influence of features with low contribution.

(2) Multi-task Loss Function

The study used Mean Squared Error (MSE) to calculate the prediction loss for the AGB and GSV tasks, respectively.

$$L_B = \frac{1}{N}\sum_{i=1}^{N}(B_i - \hat{B}_i)^2 \quad (3)$$

$$L_V = \frac{1}{N}\sum_{i=1}^{N}(V_i - \hat{V}_i)^2 \quad (4)$$

Here, B_i and V_i represent the observed AGB and GSV of the i-th sample, respectively; $\hat{B}_i$ and $\hat{V}_i$ represent the model-predicted values, respectively; and N represents the number of samples.

Because the two prediction tasks—AGB and GSV—differ in terms of their numerical ranges and optimization complexity, this study employs a weighted approach to construct a multi-task joint loss function:

$$L_{MT} = \omega_B L_B + \omega_V L_V \quad (5)$$

In this context, ω_B and ω_V represent the loss weights for the AGB and GSV tasks, respectively. The study determined these weights based on the average ratio of AGB to GSV across all sample plots. The weights were set to, setting ω_B = 1 and ω_V = 1.4 according to this average ratio, with the aim of balancing the optimization contributions of the two tasks during training.

(3) Ecological Relationship Constraints

Different forest types differ in characteristics such as species composition and wood density, and consequently, the relationship between AGB and GSV also varies among forest types. Therefore, fitting the relationships separately for different forest types may result in different relationship parameters. Considering that the objective of this study is to establish an empirical relationship that characterizes the overall association between AGB and GSV at the regional scale, rather than to develop an AGB and GSV conversion relationship for a specific forest type, we jointly fitted the paired AGB and GSV observations from all forest plots to obtain an overall empirical relationship at the regional scale, which was then incorporated into the model as an ecological constraint [39,40], as shown in Figure 3. The pooled data showed a good fit (R^2 = 0.87, RSE = 46.02, $p < 0.001$, n = 127), indicating a strong regional relationship between AGB and GSV. Because several of the 17 forest types contained only one or two sample plots, a formal statistical test of the equality of coefficients among forest types could not be reliably performed. Furthermore, fitting separate relationships for these sparsely sampled forest types would yield unstable coefficient estimates. Therefore, this study used the pooled relationship to characterize the overall regional association rather than developing separate conversion relationships for individual forest types. The empirical relationship between AGB and GSV was established using all 127 sample plots to characterize their regional-scale relationship.

First, a regional-scale univariate empirical relationship between AGB and GSV was fitted using the paired observations from the field plots:

$$B = aV + b \quad (6)$$

Here, a and b represent the slope and intercept of the linear model, respectively, and $\hat{V}$ denotes the GSV predicted by the final model. denotes the GSV predicted by the final model. The corresponding biomass under ecological constraints is calculated based on the accumulated amount predicted by the model:

$$\hat{B}_{eco} = a\hat{V} + b \quad (7)$$

The ecological constraint loss is constructed based on the difference between the estimated biomass values and the predicted biomass-ecological relationship:

$$L_{eco} = \frac{1}{N}\sum_{i=1}^{N}[\hat{B}_i - (a\hat{V}_i + b)]^2 \quad (8)$$

Finally, by incorporating the ecological constraint into the multi-task loss function, we obtain the model's total loss:

$$L_{MT} = \omega_B L_B + \omega_V L_V + \lambda_{eco} L_{eco} \quad (9)$$

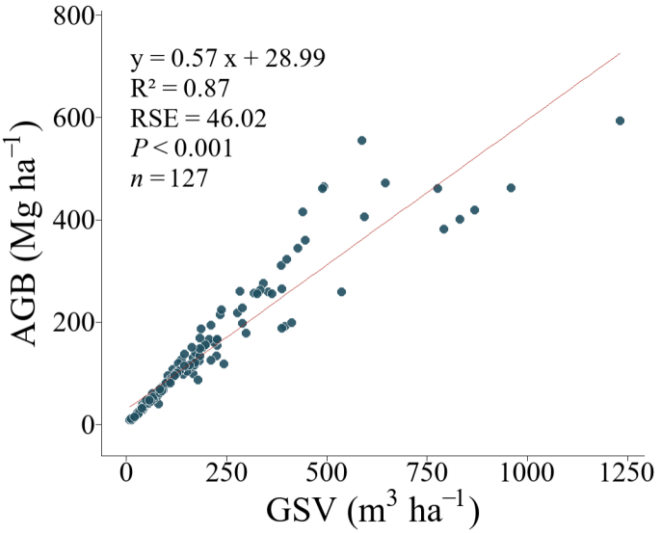


Figure 3. AGB–GSV relationship across all forest plots.

The ecological constraint coefficient was set to λ_{eco} = 0.3 based on a preliminary sensitivity analysis (Table 3). Within the tested range (0.1–0.3), model performance improved as λ_{eco} increased, and λ_{eco} = 0.3 gave the best AGB accuracy (R^2 = 0.58, RMSE = 87.37 Mg ha^{-1}) while GSV performance remained comparable to that without the constraint (λ_{eco} = 0). Larger values were not adopted because they may over-constrain the model and suppress task-specific information.

Table 3. Sensitivity analysis of loss weight ratio and ecological constraint coefficient (λ).

Weight Ratio	λ	GSV R^2	RMSE (m^3 ha^{-1})	AGB R^2	RMSE (Mg ha^{-1})
1:1.4	0	0.64 ± 0.11	132.85 ± 19.96	0.57 ± 0.10	88.21 ± 13.57
1:1.4	0.1	0.63 ± 0.11	134.88 ± 21.31	0.57 ± 0.10	88.32 ± 14.62
1:1.4	0.2	0.64 ± 0.09	133.17 ± 21.04	0.57 ± 0.09	88.24 ± 13.80
1:1.4	0.3	0.64 ± 0.08	132.99 ± 19.96	0.58 ± 0.07	87.37 ± 13.10
1:1.5	0	0.64 ± 0.11	132.97 ± 20.00	0.57 ± 0.10	88.20 ± 13.54
1:1.5	0.1	0.64 ± 0.10	133.83 ± 21.60	0.58 ± 0.10	87.44 ± 14.69
1:1.5	0.2	0.63 ± 0.11	135.95 ± 24.70	0.56 ± 0.09	89.70 ± 13.95
1:1.5	0.3	0.63 ± 0.10	135.51 ± 20.04	0.56 ± 0.10	89.23 ± 14.98
1:1.6	0	0.64 ± 0.11	133.17 ± 19.89	0.57 ± 0.10	88.20 ± 13.44
1:1.6	0.1	0.63 ± 0.11	135.43 ± 22.88	0.56 ± 0.09	88.95 ± 13.42
1:1.6	0.2	0.62 ± 0.11	136.24 ± 24.63	0.56 ± 0.09	89.76 ± 13.83
1:1.6	0.3	0.63 ± 0.10	135.41 ± 19.85	0.56 ± 0.10	88.90 ± 14.98

2.4.2. Validation of Model Validity

The proposed model was evaluated for the joint prediction of forest AGB and GSV through four analyses: feature selection, architectural ablation, sensitivity assessment, and benchmarking against alternative methods. Furthermore, SHAP analysis was employed to interpret the model's predictions and examine the relative contributions of individual variables to AGB and GSV estimation.

The feature selection ablation experiment was designed to address potential information redundancy between remote sensing data and environmental variables and to analyze the impact of different combinations of input variables on model performance. First, the importance of each input variable in the AGB and GSV tasks was calculated using a random forest model, and three feature input schemes were constructed: the feature set for the AGB task, the feature set for the GSV task, and the shared feature set based on the combined contributions of both tasks. Based on the identification of the optimal combination of input features, the model structure ablation experiments were further conducted to evaluate the impact of different functional modules on the model's predictive performance. Taking the basic MLP model as the baseline, the study progressively introduces multi-task learning mechanisms, attention mechanisms, and ecological relationship constraints to construct four model architectures: MLP, multi-task-MLP, attention-multi-task-MLP, and ecological attention-multi-task-MLP. The MLP was used to learn nonlinear relationships and combinations among the input variables through fully connected layers**.** The ten input variables were arranged according to their RF importance from high to low. This ordering was used to construct a fixed feature sequence and does not represent actual spatial proximity among the variables. The prediction results of different model architectures were compared to analyze the contributions of task-sharing mechanisms, dynamic feature weighting strategies, and ecological prior constraints to model optimization performance. In addition, given the limited number of field plots, feature selection and model structure ablation experiments were conducted to investigate the contributions of different model components to predictive performance. Given that the study relied on a dataset of only 127 field plots, we conducted feature selection and model structure ablation experiments to investigate the contribution of various model components to predictive performance. Furthermore, we comprehensively evaluated the proposed model by comparing it with Random Forest (RF) [41], Extreme Gradient Boosting (XGBoost) [42], K-Nearest Neighbors (KNN) [43], and Categorical Boosting (CatBoost) [44]. By comparing the prediction results, we further explored the relationship between model complexity and predictive performance, while also analyzing the proposed model's applicability under the current sample conditions and its potential risk of overfitting. All models were trained using the same training–test splitting strategy, set of input variables, and evaluation metrics. Feature selection and the AGB–GSV relationship were deliberately determined from the full set of plots to define a common input set and a regional ecological prior; the test set was not used for model fitting, tuning, or model selection. For MLP, the architecture and hyperparameter settings were determined as the basic configuration for subsequent MLP-based model development, rather than being independently optimized for baseline comparison. Since GSV can be used to estimate AGB, a baseline experiment was conducted by first predicting GSV using the Eco-AMT-MLP model and then converting the predicted GSV to AGB using the empirical linear relationship between AGB and GSV. All models were run on Python 3.7. The key parameter settings for the different models are shown in Table 4.

Table 4. Model Parameter Settings.

Model	Hyperparameter Settings
RF	n_estimators = 500; max_features = default; other parameters = default
XGBoost	n_estimators = 500; learning rate = 0.01; max_depth = 6; other parameters = default
KNN	n_neighbors = 5; distance metric = Euclidean
CatBoost	iterations = 300; learning rate = 0.03; depth = 5; random seed = 123–132; other parameters = default
MLP	Linear(10,64) + Linear(64,32) + Linear(32,2); activation = ReLU; dropout = 0.3; optimizer = Adam; learning rate = 0.0001; batch size = 32; maximum epochs = 2000; weight decay = 1×10^{-4}; trainable parameters = 2850
MultiTask-MLP	Shared feature layers: Linear(10,64) + Linear(64,32); two task-specific output heads; activation = ReLU; dropout = 0.3; optimizer = Adam; learning rate = 0.0001; batch size = 32; maximum epochs = 2000; weight decay = 1×10^{-4}; task loss weights = (1, 1.4); trainable parameters = 2850
Attention-MultiTask-MLP	MultiTask-MLP + sigmoid attention module; other settings consistent with MultiTask-MLP; trainable parameters = 2960
Eco-Attention-MultiTask-MLP	Attention-MultiTask-MLP + ecological constraint loss; $\lambda = 0.3$; task loss weights = (1, 1.4); trainable parameters = 2960

Note: The conventional machine-learning models were run with default or lightly specified hyperparameters and were not systematically tuned; they are therefore used as reference points rather than as tuned competitors.

2.4.3. Model Evaluation

To evaluate the predictive performance of the Eco-AMT-MLP model, the 127 field plots were randomly divided into training and test sets at a ratio of 7:3, with an initial random seed of 123. Ten random data splits were performed using different random seeds. For each split, the model was trained using the training set, and its predictive performance was evaluated using the test set. The coefficient of determination (R^2) and root mean square error (RMSE) were used to evaluate model performance, and the mean values of the results from the 10 experiments were calculated. The interval distributions of the training and test samples across the 10 random splits are shown in Figure 4.

$$R^2 = 1 - \frac{\sum_{i=1}^{N}(y_i - \hat{y}_i)^2}{\sum_{i=1}^{N}(y_i - \bar{y})^2} \tag{10}$$

$$RMSE = \sqrt{\frac{\sum_{i=1}^{N}(y_i - \hat{y}_i)^2}{N}} \tag{11}$$

where N is the number of sample observations, y_i is the actual AGB value, $\hat{y}_i$ is the estimate, and $\bar{y}_i$ is the average AGB of the observed samples.

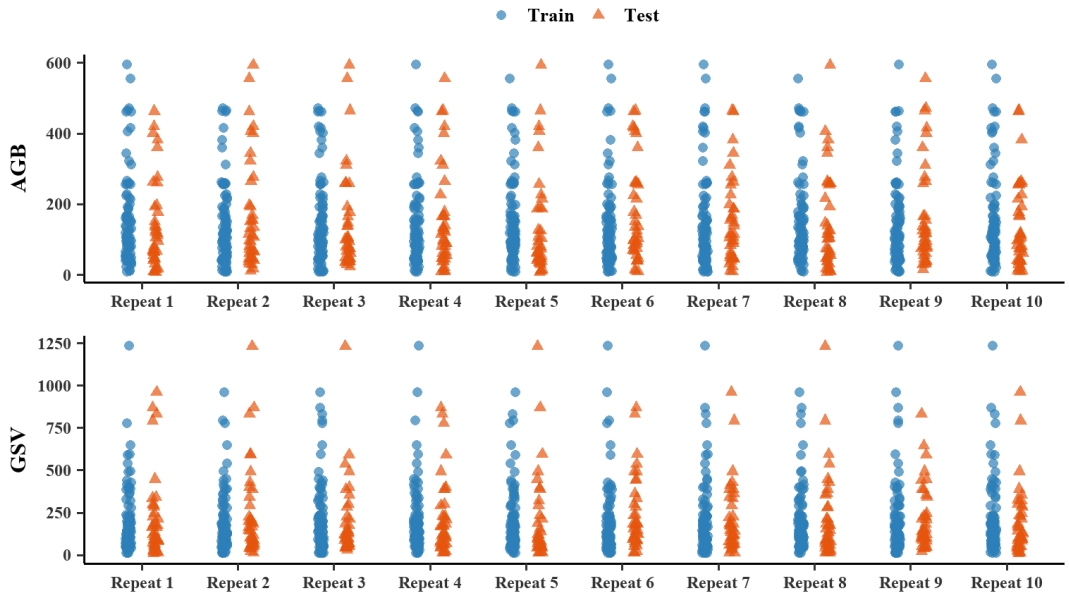


Figure 4. Distributions of training and test samples for GSV and AGB across 10 random 7:3 splits.

https://doi.org/10.3390/f17111318

3. Results

3.1. Results of Variable Selection

Random Forest (RF)-based importance scores were calculated to identify the key predictors for AGB estimation, GSV estimation, and the common predictor set used for both tasks (Figure 5). Key variables for AGB were primarily spectral and soil-related, with B8, CEC, and B11 showing high importance. Key variables for GSV mainly comprised spectral and topographic features, with B8, B11, B6, and B8a demonstrating high importance. Within the set of shared variables, spectral features exhibited the highest overall importance, particularly B8, B11, and B6. Topographic and soil features also made notable contributions. The final selection of shared variables included five spectral features (B6, B8, B8a, and B11), two topographic features (DEM and Aspect), and four soil features (CEC, SOC, Sand, Silt).

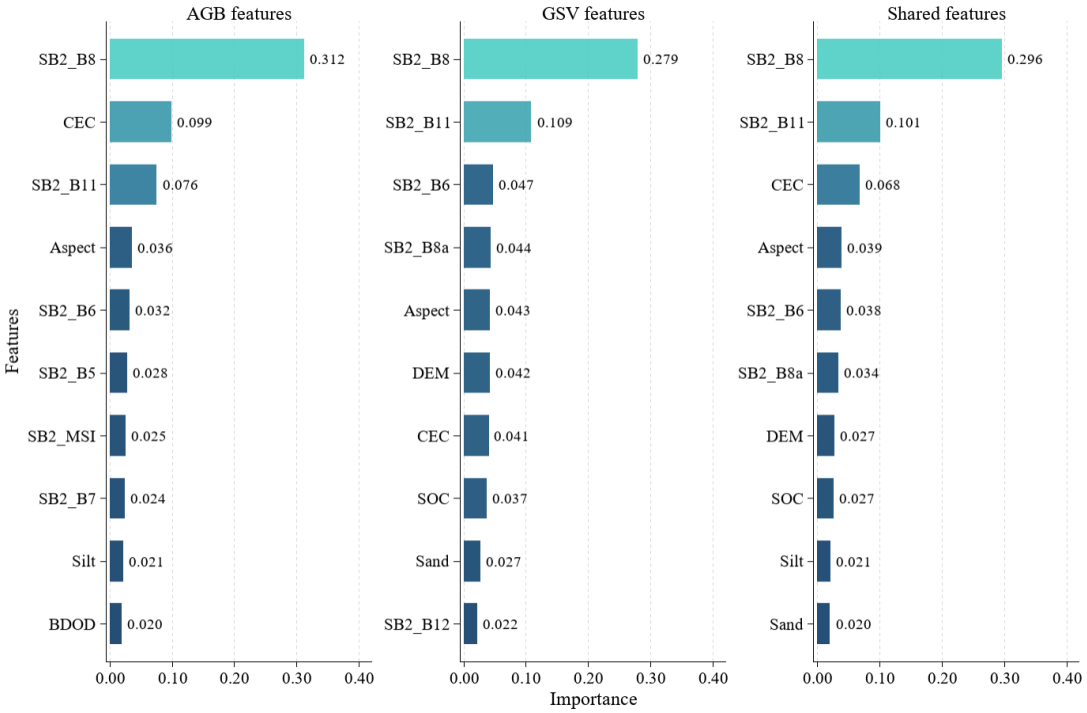


Figure 5. Feature selection results for the two approaches.

3.2. Model Evaluation and Sensitivity Analysis

Table 3 shows that variations in the task weight ratio and ecological constraint coefficient (λ) had a limited effect on model performance. Across the 12 parameter combinations, GSV R^2 ranged from 0.62 to 0.64, with RMSE ranging from 132.85 to 136.24 m^3 ha^{-1}. For AGB, R^2 ranged from 0.56 to 0.58, while RMSE ranged from 87.37 to 89.76 Mg ha^{-1}. These results indicate that model performance was relatively stable across different loss weight settings. Under the task weight ratio of 1:1.4, both GSV and AGB prediction performance generally improved as λ increased from 0.1 to 0.3. At $\lambda = 0.3$, GSV achieved an R^2 of 0.64 ± 0.08 and an RMSE of 132.99 ± 19.96 m^3 ha^{-1}, while AGB achieved an R^2 of 0.58 ± 0.07 and an RMSE of 87.37 ± 13.10 Mg ha^{-1}. This combination yielded the highest mean AGB R^2 and the lowest mean AGB RMSE among all tested settings, while its GSV performance was comparable to the best-performing configuration ($R^2 = 0.64$ and RMSE = 132.85 m^3 ha^{-1} at $\lambda = 0$). Although $\lambda = 0$ produced a marginally lower GSV RMSE, the combination of a 1:1.4 task weight ratio and $\lambda = 0.3$ provided a balanced performance across the two prediction tasks. Therefore, this combination was selected for the final model.

Under the present hyperparameter settings, the Eco-AMT-MLP model achieved the highest mean R^2 and lowest mean RMSE among the compared models for both GSV and AGB prediction, excluding the GSV-to-AGB conversion baseline from this comparison, as illustrated in Figure 6. Since the baseline models were not tuned with the same intensity, this comparison should be regarded as a relative indication rather than a definitive ranking. Using 10 repeated random 7:3 train–test splits, this model reached an R^2 of 0.64 ± 0.08 and an RMSE of 132.99 ± 19.96 m^3 ha^{-1} for GSV, together with an R^2 of 0.58 ± 0.07 and an RMSE of 87.37 ± 13.10 Mg ha^{-1} for AGB. Relative to the other models, Eco-AMT-MLP also provided more consistent predictions for samples with high GSV values, although underestimation still occurred to some extent in this range. The MLP obtained R^2 values of 0.60 ± 0.10 for GSV and 0.47 ± 0.11 for AGB, with corresponding RMSE values of 140.45 ± 19.17 and 97.49 ± 9.31. Among the conventional machine-learning approaches, XGBoost performed relatively well, yielding R^2 values of 0.59 ± 0.11 for GSV and 0.54 ± 0.11 for AGB. RF produced R^2 values of 0.57 ± 0.13 and 0.53 ± 0.12, respectively. CatBoost gave R^2 values of 0.59 ± 0.10 for GSV and 0.50 ± 0.09 for AGB. KNN showed weaker predictive ability, especially for AGB, with an R^2 of 0.36 ± 0.08 and an RMSE of 107.64 ± 9.52 Mg ha^{-1}. The GSV-based AGB prediction baseline reached an R^2 of 0.57 ± 0.10 and an RMSE of 88.62 ± 14.07 Mg ha^{-1}. These results indicate that Eco-AMT-MLP achieved AGB estimation performance comparable to that of the GSV-to-AGB conversion baseline, whereas its GSV predictions showed stronger performance than those of the independent MLP and conventional machine-learning models. In general, Eco-AMT-MLP maintained a higher mean R^2 and a lower RMSE than the independent MLP and most conventional machine-learning models over the repeated experiments.

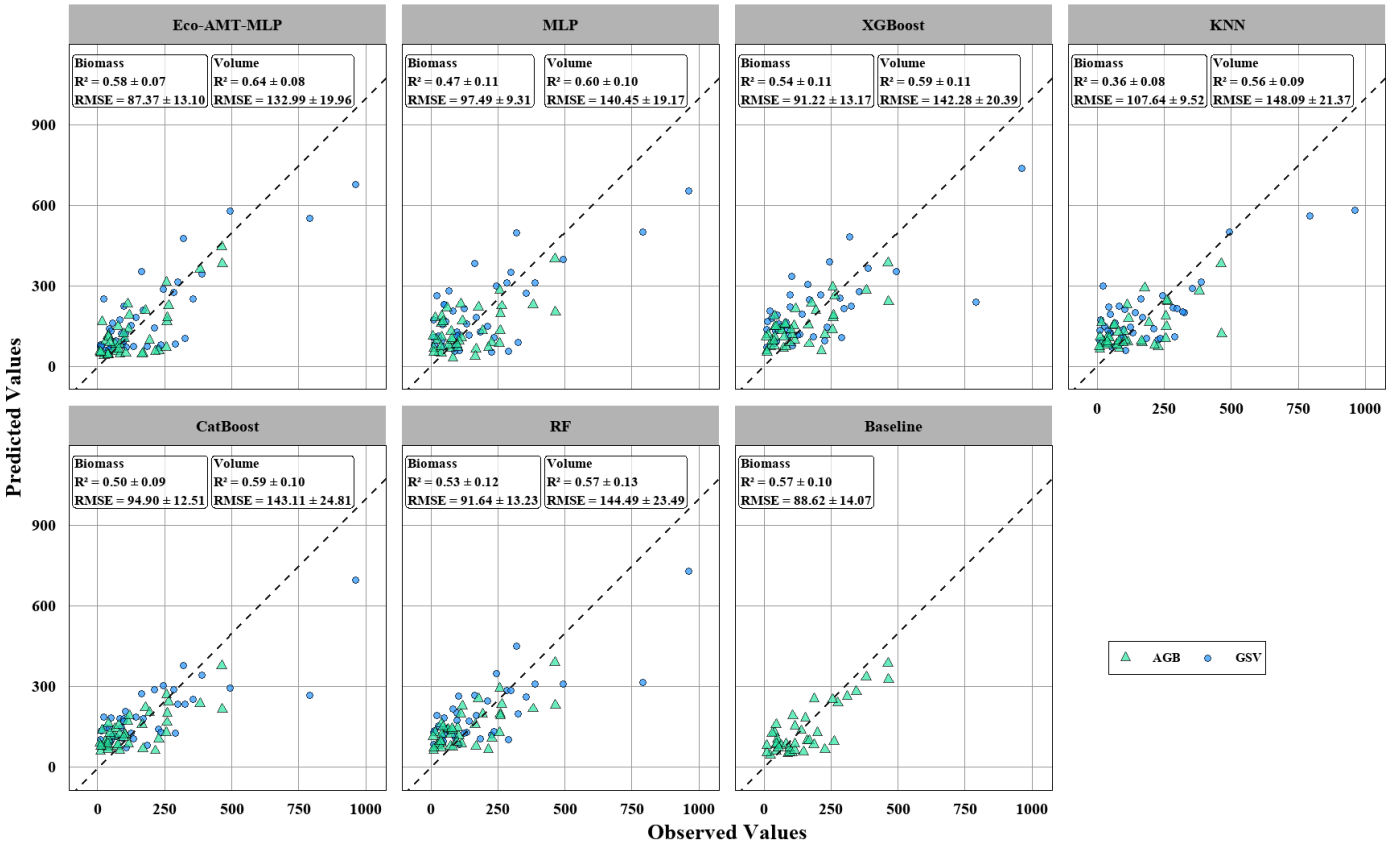


Figure 6. Scatter plots of forest AGB and GSV for different models. Note: Across 10 random data splits, Eco-AMT-MLP outperformed XGBoost in GSV R^2 and RMSE in 8 splits each, and in AGB R^2 and RMSE in 6 splits each; compared with the conversion baseline, it outperformed the baseline in AGB in 6 splits.

3.3. Comparison of Model Performance and Analysis of Feature Selection

Table 5 shows that the MLP model reached R^2 values of 0.60 ± 0.10 for GSV and 0.47 ± 0.11 for AGB, with RMSE values of 140.45 ± 19.17 m^3 ha^{-1} and 97.49 ± 9.31 Mg ha^{-1}, respectively. Table 5 reports the stepwise ablation, in which each row adds one component to the previous architecture, allowing the contribution of multi-task learning, attention, and the ecological constraint to be examined separately. With the introduction of multi-task learning, AGB estimation improved, as indicated by R^2 values of 0.60 ± 0.11 for GSV and 0.54 ± 0.10 for AGB, together with RMSE values of 140.99 ± 20.54 m^3 ha^{-1} and 91.35 ± 12.69 Mg ha^{-1}, respectively. These findings suggest that shared feature learning alone did not notably enhance GSV estimation, although it did improve AGB estimation. When the attention mechanism was added, the Attention-MultiTask-MLP attained R^2 values of 0.64 ± 0.10 for GSV and 0.56 ± 0.09 for AGB, along with RMSE values of 133.21 ± 21.02 m^3 ha^{-1} and 89.04 ± 13.94 Mg ha^{-1}, respectively. Compared with the MLP model, the R^2 values rose by 0.04 for GSV and 0.09 for AGB, whereas the RMSE values declined by 7.24 m^3 ha^{-1} and 8.45 Mg ha^{-1}, respectively. These gains imply that the attention mechanism strengthened the model's capacity to recognize and exploit informative input features. After the ecological constraint was further integrated, the Eco-Attention-MultiTask-MLP delivered the best overall performance, with R^2 values of 0.64 ± 0.08 for GSV and 0.58 ± 0.07 for AGB, and RMSE values of 132.99 ± 19.96 m^3 ha^{-1} and 87.37 ± 13.10 Mg ha^{-1}, respectively. Relative to the MLP model, the R^2 values increased by 0.04 for GSV and 0.11 for AGB, while the RMSE values decreased by 7.46 m^3 ha^{-1} and 10.12 Mg ha^{-1}, respectively. The further gain in AGB estimation suggests that embedding the ecological relationship between GSV and AGB may have imposed an additional constraint during model optimization, thereby helping the model achieve more accurate joint estimation of the two forest parameters. However, it should be noted that the improvements contributed by individual components are not uniform across tasks, and some differences between successive architectures are relatively small.

Among the different feature selection strategies, the Shared_average feature set achieved the best overall performance for both GSV and AGB estimation (Table 6). The GSV_only feature set obtained R^2 values of 0.63 ± 0.10 and 0.55 ± 0.11, with RMSE values of 133.39 ± 20.18 m^3 ha^{-1} and 89.67 ± 13.33 Mg ha^{-1} for GSV and AGB, respectively. The AGB_only feature set showed lower performance, with R^2 values of 0.51 ± 0.12 and 0.47 ± 0.01 and RMSE values of 155.37 ± 28.85 m^3 ha^{-1} and 96.82 ± 10.50 Mg ha^{-1} for GSV and AGB, respectively. In contrast, the Shared_average feature set achieved R^2 values of 0.64 ± 0.08 for GSV and 0.58 ± 0.07 for AGB, with RMSE values of 132.99 ± 19.96 m^3 ha^{-1} and 87.37 ± 13.10 Mg ha^{-1}, respectively. These results suggest that integrating informative variables from both tasks provides more comprehensive information for joint GSV and AGB estimation.

Table 5. Comparison of the Predictive Performance of AGB and GSV Across Different Model Modules.

Model	GSV R^2	GSV RMSE	AGB R^2	AGB RMSE
MLP	0.60 ± 0.10	140.45 ± 19.17	0.47 ± 0.11	97.49 ± 9.31
MultiTask-MLP	0.60 ± 0.11	140.99 ± 20.54	0.54 ± 0.10	91.35 ± 12.69
Attention-MultiTask-MLP	0.64 ± 0.10	133.21 ± 21.02	0.56 ± 0.09	89.04 ± 13.94
Eco-Attention-MultiTask-MLP	0.64 ± 0.08	132.99 ± 19.96	0.58 ± 0.07	87.37 ± 13.10

Note: Across 10 identical random data splits, Eco-AMT-MLP outperformed MLP, MultiTask-MLP, and Attention-MultiTask-MLP in GSV R^2 and RMSE in 8 splits each, and in AGB R^2 and RMSE in 7, 6, and 8 splits, respectively.

Table 6. Prediction performance of AGB and GSV using different feature sets.

Method	GSV R^2	GSV RMSE	AGB R^2	AGB RMSE
GSV_only	0.63 ± 0.10	133.39 ± 20.18	0.55 ± 0.11	89.67 ± 13.33
AGB_only	0.51 ± 0.12	155.37 ± 28.85	0.47 ± 0.10	96.82 ± 10.50
Shared_average	0.64 ± 0.08	132.99 ± 19.96	0.58 ± 0.07	87.37 ± 13.10

3.4. SHAP-Based Explainability Analysis

The SHAP approach was used to quantify the effects of different input variables on the Eco-AMT-MLP model outputs for AGB and GSV, as illustrated in Figure 7. The results indicate that SB2_B11, Silt, and SOC exhibit the highest mean absolute SHAP values across both tasks SB2_B11 = 18.76 for AGB and 29.12 for GSV), signifying their substantial contribution to the model's predictions. DEM, SB2_B8, and Aspect also demonstrate significant contributions, whereas Sand, SB2_B6, and CEC show relatively lower mean absolute SHAP values. The SHAP values are distributed across both positive and negative ranges, suggesting that the direction of a specific variable's contribution to the prediction results may vary across different samples. The SHAP value distributions for SB2_B11, SOC, and DEM are wide, indicating marked variation in the magnitude of their contributions across samples. In contrast, the SHAP value distributions for soil variables (CEC) are relatively concentrated, implying minimal variation in the magnitude of their contributions to the prediction results across different samples. In contrast, the SHAP value distributions for soil variables (CEC) are relatively concentrated, implying minimal variation in the magnitude of their contributions to the prediction results across different samples.

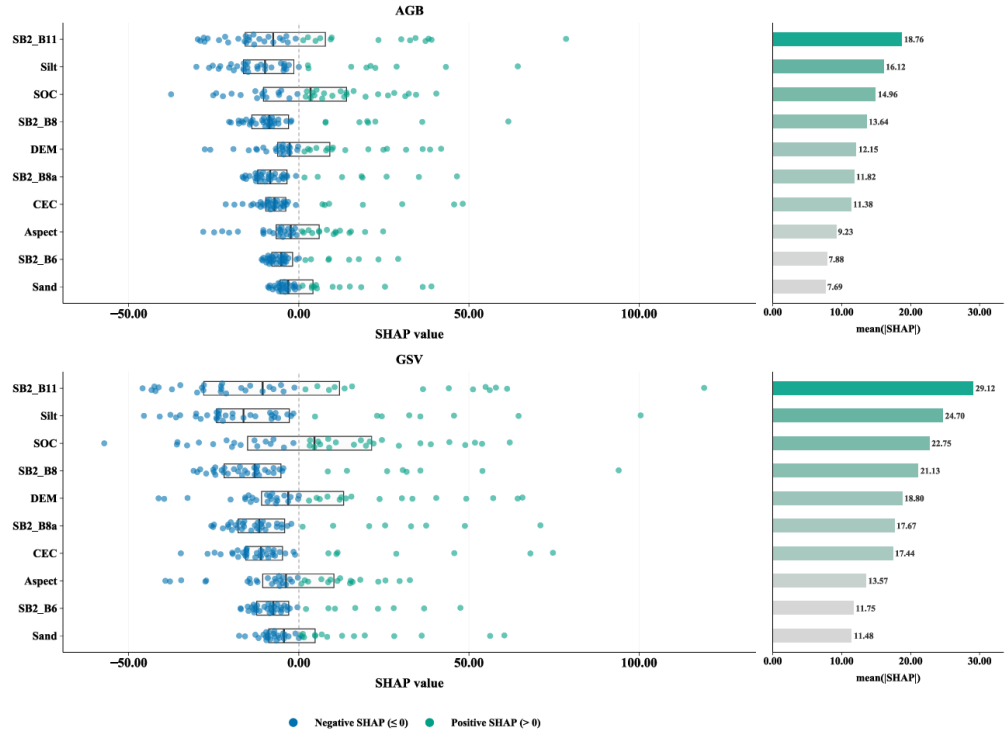


Figure 7. SHAP Feature Importance and Contribution Analysis of the Eco-AMT-MLP.

3.5. Forest AGB and GSV Inversion

Figure 8 shows the spatial distributions of forest AGB and GSV predicted by the Eco-AMT-MLP and XGBoost models. Compared with XGBoost, the Eco-AMT-MLP predictions show more continuous spatial patterns, smoother spatial gradients, and greater local spatial variation. High-resolution OMAP satellite imagery acquired in March 2021 was used as supplementary background imagery to provide a spatial reference for forest

distribution in the study area and facilitate the visualization and interpretation of the predicted AGB and GSV maps. In comparison, the XGBoost predictions show relatively limited spatial variation in some low-value areas and a relatively large area of high predicted GSV. These visual comparisons provide qualitative information on the spatial patterns of the two models.

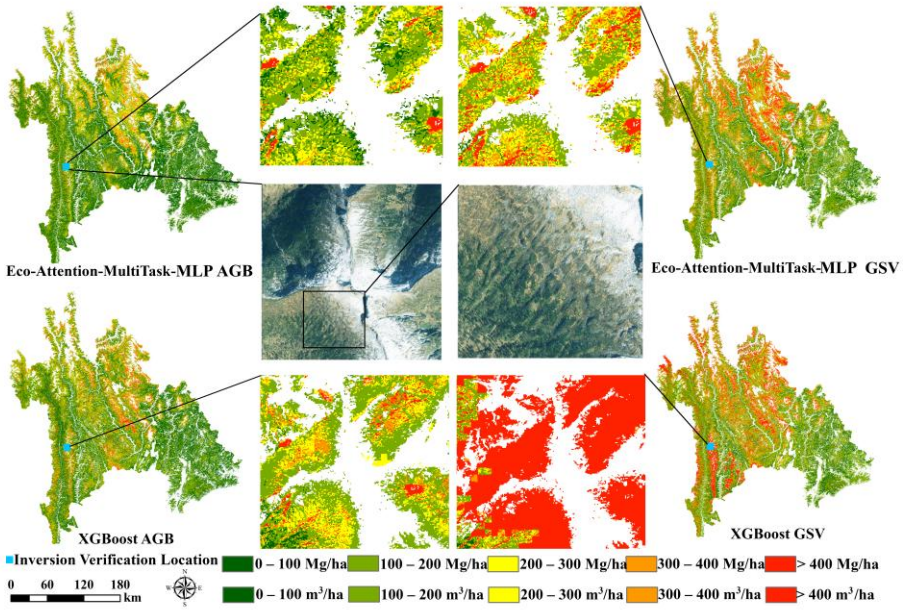


Figure 8. Inversion plots of forest AGB and GSV for the Eco-AMT-MLP and XGBoost models.

4. Discussion

4.1. Variable Selection and Key Predictors of Forest GSV and AGB

Selecting appropriate variables is a crucial procedure when estimating forest aboveground biomass (AGB) and growing stock volume (GSV) from remote sensing data. The selected features in this study included Sentinel-2 spectral, topographic, and soil variables, with spectral bands such as B8 and B11 playing important roles. Their contribution is biologically plausible because Sentinel-2 spectral observations are sensitive to canopy moisture and vegetation structure [45]. In addition to spectral variables, topographic factors such as DEM and aspect were also identified as significant variables. The terrain in northwestern Yunnan is quite rugged, and variations in elevation and slope aspect affect local temperature, moisture, and vegetation growth conditions, which in turn influence forest structure [46]. Previous studies of forest AGB in mountainous areas have also found that topographic variables such as elevation, slope, and aspect can explain some of the spatial variation in forest AGB and GSV [47]. Additionally, soil variables such as CEC, SOC, and sand content were included in the set of key features. This is because SOC, CEC, and soil texture reflect soil nutrient availability and water-holding capacity, which in turn influence forest AGB and GSV [48]. However, the climate factor was not included in the final feature set. This may be because some of its information overlaps with that of the topography and soil factors, resulting in a lower contribution during variable selection [49]. Predictor composition differed between the task-specific feature sets, indicating that AGB and GSV may not respond identically to environmental information. GSV primarily reflects the volume of wood in a forest stand, whereas AGB is additionally influenced by tree species composition and wood density [50]. Therefore, the contributions of these two variables differ. The Shared average feature set retains key variables from both tasks, allowing for the integrated use of spectral, topographic, and soil information, thereby

reducing the loss of information that might result from selecting variables based on a single objective. Overall, the contributions of variables vary across different feature sets, while Shared average provides more comprehensive information for predicting GSV and AGB by integrating key variables from multiple sources.

4.2. Model Optimization and Multi-Task Feature Selection

The Eco-AMT-MLP achieved the best performance in both GSV and AGB estimation. This advantage may reflect the ability of the MLP to learn hierarchical feature interactions within a shared representation, whereas traditional machine learning models have relatively limited capabilities for modeling interactions among high-dimensional features [13]. However, the baseline approach, which first predicts GSV and then converts it to AGB, achieved nearly identical AGB prediction accuracy (R^2 = 0.57 ± 0.10, RMSE = 88.62 ± 14.07) to that of the proposed model (R^2 = 0.58 ± 0.07, RMSE = 87.37 ± 13.10), suggesting that the improvement in AGB estimation primarily stems from the empirical coupling between GSV and AGB rather than the multi-task architecture itself. Nevertheless, the primary contribution of our multi-task architecture lies in the direct estimation of GSV, as Eco-AMT-MLP achieved the highest GSV accuracy (R^2 = 0.64 ± 0.08) among all models, which subsequently ensures the reliability of the converted AGB. Compared to a single MLP, the introduction of multi-task learning resulted in only a slight change in performance, indicating that simple feature sharing struggles to fully leverage the complementary information across tasks. After incorporating the attention mechanism into the MultiTask-MLP, the R^2 values for GSV and AGB increased by 0.04 and 0.02, respectively, while the RMSE values decreased by 7.78 m^3 ha^{-1} and 2.31 Mg ha^{-1}, respectively. With the further incorporation of the ecological constraint, the R^2 value for GSV remained unchanged, whereas that for AGB increased by 0.02. Meanwhile, the RMSE values decreased by 0.22 m^3 ha^{-1} for GSV and 1.67 Mg ha^{-1} for AGB. These results indicate that the attention mechanism substantially improved GSV estimation, while the ecological constraint provided additional improvements, particularly for AGB estimation. Xu et al. [23] incorporated biological compatibility into the neural network loss function, resulting in a decrease in the AGB prediction RMSE from 166.864 kg to 154.860 kg, demonstrating that ecological relationship constraints can effectively improve the predictive performance of machine learning models. From the predictive performance of different models, the differences between Eco-AMT-MLP and the other models were generally moderate, and the models exhibited similar trends in predictive performance, indicating that Eco-AMT-MLP achieved relatively stable predictive performance. The effects of the ecological constraint varied across estimation tasks. Previous studies have shown that incorporating biological compatibility into the neural network loss function can improve AGB estimation accuracy and consistency among AGB components [23]. Furthermore, studies on forest AGB have shown that incorporating spatial information can reduce prediction variance [51]. Across the 10 random data splits, Eco-AMT-MLP exhibited a lower standard deviation in R^2 than the other models, indicating relatively stable predictive performance across different data splits. The lower standard deviation in R^2 also suggests that its fitting performance was relatively stable. However, its RMSE standard deviation was not the lowest among all models, which may be related to differences in the distribution of prediction errors across data splits. Because RMSE is sensitive to changes in the magnitude and distribution of errors, it may still fluctuate to some extent even when the model exhibits relatively stable overall fitting performance [52]. Compared with MLP, Eco-AMT-MLP increased the mean R^2 by 0.11 for AGB estimation and by 0.04 for GSV estimation. The former was comparable to the standard deviation of MLP's R^2 (0.11), whereas the latter was smaller than the standard deviation (0.10), indicating that the magnitude of performance improvement relative to the variability across different data splits differed between the two tasks. The accuracy of forest AGB estimation from remote sensing is influenced by factors such as remote sensing data,

stand structure, and modeling methods, while GSV prediction is also subject to uncertainties associated with environmental covariates [53]. These factors may lead to differences in the effects of ecological constraints on AGB and GSV estimation, resulting in different magnitudes of performance improvement between the two tasks. Nevertheless, the AGB estimation performance of Eco-AMT-MLP ($R^2 = 0.58 \pm 0.07$; RMSE = 87.37 ± 13.10 Mg ha^{-1}) indicates that considerable uncertainty remains. Previous studies using LiDAR and multi-source remote sensing data have reported varying levels of AGB estimation accuracy, reflecting differences in forest conditions, data sources, and validation strategies [3,54]. Although Eco-AMT-MLP performed well relative to the models evaluated in this study, an R^2 of 0.58 may be insufficient for applications requiring precise plot-level AGB estimates. The final model also showed more stable predictions for high-value samples. This pattern may reflect the combined effects of multi-source feature integration and ecological regularization, which could help constrain predictions for extreme observations [55].

Single-task feature sets can highlight variables relevant to the target, but may result in the loss of some useful information [38]. Feature selection depends not only on the degree of correlation between the variables and the target, but also on how well the selected features align with the model's learning task [56]. In this study, the GSV-only feature set performed well in GSV prediction, while the AGB-only feature set showed a significant decline in performance for GSV prediction, reflecting the bias inherent in single-task feature selection. The shared average combines the feature contributions from both tasks, improving the alignment between the features and the multi-task objectives. Xiang et al. [57] employed a shared feature extraction network to integrate various types of forest structural information and simultaneously predict multiple biophysical parameters of forest stands, demonstrating that shared features can provide effective information representation for relevant forest parameters. Qin et al. [24] used shared LSTM layers and multi-task learning to simultaneously predict the AGB of different forest organs and total AGB, demonstrating that shared feature representations can effectively utilize the inter-task correlation information.

4.3. Ecological Mechanisms Underlying Feature Contribution

SHAP analysis revealed the contribution and importance of different variables to the model predictions. SB2_B11, Silt, and SOC showed the highest feature importance across both tasks, with mean |SHAP| values of 18.76, 16.12, and 14.96 for AGB (and 29.12, 24.70, and 22.75 for GSV, respectively). The dominance of SB2_B11 can be mainly attributed to the sensitivity of the short-wave infrared (SWIR) band to vegetation water content, canopy structure, and biogeochemical characteristics [58]. The high ranking of Silt and SOC highlights the critical role of soil texture and soil organic carbon in regulating nutrient availability, water retention, and forest productivity [59]. DEM also ranked relatively high in importance (12.15 for AGB and 18.80 for GSV), implying that topography contributes importantly to forest growth by shaping hydrothermal regimes and resource allocation [4]. SB2_B8 and Aspect also showed considerable mean absolute SHAP values (11.82 and 9.23 for AGB, respectively), indicating substantial contributions to model predictions. In contrast, CEC (11.38 for AGB and 17.44 for GSV), SB2_B6, and Sand had relatively lower mean absolute SHAP values. Their lower contributions do not necessarily imply limited ecological importance, as correlated predictors may contain overlapping information. The SHAP value distributions of SB2_B11, SOC, and DEM were relatively broad, indicating substantial variation in their effects on model predictions across samples [60].

4.4. Limitations and Future Directions

Although the Eco-AMT-MLP developed in this study achieved good predictive performance in estimating forest AGB and GSV, it still has certain limitations. Considering

the spatial heterogeneity of forest ecosystems, all 127 plots were used for RF-based feature selection and AGB–GSV relationship fitting to characterize regional patterns. However, this approach may affect the independence of model evaluation. In addition, some hyperparameters were selected with reference to test-set performance, which may introduce model selection bias and lead to optimistic estimates of predictive performance. Future studies should perform feature selection and AGB–GSV relationship fitting exclusively within each training subset and select hyperparameters using an internal validation set, while reserving the test set for final evaluation. Furthermore, the random splitting of plots did not explicitly account for spatial autocorrelation, which may affect the independence of model evaluation. In this study, AGB and GSV were compiled from the same tree measurements, so their linear relationship largely reflects how the data were compiled rather than a purely ecological relationship. In addition, the pooled regression systematically overestimates AGB for over-mature *Abies*/*Picea* stands with GSV > 750 m^3 ha^{-1} (residuals of −629 to −1138 for six plots, reflecting their low wood density); because several forest types have too few samples ($n \leq 4$) for separate fits, this bias should be noted when applying the model to high-GSV over-mature conifer stands. Future studies should adopt spatially blocked validation to better assess model generalizability. Due to the limited sample size and spatial coverage of the study, the model was primarily trained using data from plot sites in northwestern Yunnan, and its generalizability across different forest types, ecological regions, and temporal scales still requires further validation. The limited number and uneven spatial distribution of sample plots may restrict the representation of forest conditions and reduce model transferability to areas with different environmental characteristics [61]. Therefore, the applicability of the proposed model to other forest regions, particularly high-elevation areas with insufficient field observations, requires further evaluation using additional field measurements and independent spatial validation. Furthermore, the model contains approximately 2900 parameters, whereas only 60–89 plots were available for training in each split. This relatively high model complexity compared with the training sample size may increase the risk of overfitting. Future studies should expand the training dataset to improve model robustness and generalizability. The baseline models (RF, XGBoost, CatBoost, and KNN) were trained using default or basic hyperparameter settings rather than being exhaustively tuned via internal cross-validation, which may have limited their optimal performance and influenced the comparative results. When the model is applied to different regions or time periods, changes in vegetation composition and environmental conditions may lead to a decline in predictive performance, thereby affecting its generalizability [62]. In addition, the sampled plots reach a maximum elevation of 4333 m, whereas the study area extends to approximately 6145 m. Although remote sensing data can support continuous retrieval in high-altitude regions, the reliability of model predictions in these areas remains to be verified, due to variations in environmental conditions and insufficient sample plot coverage. Future work will incorporate additional sample plots from high-altitude regions to enhance the model's generalization capability. Additionally, Sentinel-2 spectral, topographic, and soil variables still have limited ability to characterize forest vertical structure. In the future, LiDAR, SAR, and multi-temporal remote sensing data could be further integrated to enhance the characterization of canopy height, vertical structure, and spatial heterogeneity within forests. The fusion of multi-source remote sensing data, including optical, SAR, and LiDAR imagery, can make use of their complementary information to strengthen the accuracy and robustness of forest AGB estimation [63]. Ecological constraints are adopted in this work to strengthen the joint estimation of GSV and AGB. However, ecological relationships are still primarily expressed through empirical equations, and the characterization of forest growth processes and biological mechanisms remains relatively limited. From a practical perspective, these limitations imply that the model should be applied

with caution in high-mountain forests and in areas outside the study region. In high-elevation stands where field plots are sparse, predictions should be treated as indicative and accompanied by local calibration or additional field verification before being used for management decisions. Similarly, when transferred to other forest areas with different species composition or environmental gradients, the model requires independent spatial validation and, where necessary, retraining with local samples. Future studies could further integrate stand structure, growth processes, and physical-ecological mechanisms to develop more biologically grounded deep learning models.

5. Conclusions

This study integrated Sentinel-2 remote sensing data with topographic and environmental factors to develop the Eco-AMT-MLP model for joint estimation of forest aboveground biomass (AGB) and growing stock volume (GSV). The model achieved R^2 values of 0.64 ± 0.08 for GSV and 0.58 ± 0.07 for AGB, with RMSE values of 132.99 ± 19.96 m^3 ha^{-1} and 87.37 ± 13.10 Mg ha^{-1}, respectively. Compared with the MLP baseline, Eco-AMT-MLP improved prediction performance for both tasks. However, its AGB estimation performance was comparable to that of the GSV-to-AGB conversion baseline, indicating that predicting GSV and subsequently applying a regional conversion equation can provide similar AGB estimates. Ablation experiments showed that the attention mechanism and ecological constraint contributed to improved prediction performance by enhancing feature representation and incorporating the ecological relationship between AGB and GSV. The shared feature set provided stable performance across both tasks, highlighting the potential value of shared information for joint estimation. Sensitivity analysis further indicated that model performance depended on the task-loss weight ratio and ecological constraint coefficient, with the selected parameter setting balancing GSV and AGB estimation. SHAP analysis identified DEM, SOC, CEC, silt, and aspect as important predictors, highlighting the relevance of topographic and soil conditions to forest resource estimation. Overall, Eco-AMT-MLP provides a framework for jointly estimating AGB and GSV by integrating remote sensing and environmental information with ecological constraints, supporting forest resource monitoring, carbon stock assessment, and ecological management in northwestern Yunnan.

Author Contributions: J.L.: Writing—review and editing, Writing—original draft, Supervision, Project administration, Funding acquisition, Formal analysis, Conceptualization. Q.H.: Formal analysis, Data curation, Conceptualization. Y.L.: Formal analysis, Data curation. Y.Y.: Writing—review and editing, Conceptualization. P.W.: Formal analysis, Conceptualization. S.L.: Formal analysis, Conceptualization. Y.S.: Data Curation, Conceptualization. W.L.: Writing—review and editing, Writing—original draft, Supervision, Project administration, Formal analysis, Conceptualization. All authors have read and agreed to the published version of the manuscript

Funding: This research was supported by the Shandong Agriculture and Engineering University (No.2024GCCZR-15).

Data Availability Statement: Data will be made available on request.

Conflicts of Interest: The authors declare that they have no known competing financial interests or personal relationships that could have appeared to influence the work reported in this paper.

Appendix A

Table A1. Distribution of sample plots by forest type and stand age.

Forest Type	Young Forest	Middle-Aged Forest	Near-Mature Forest	Mature Forest	Over-Mature Forest	Total
Conifer–broadleaf mixed forest	5	7	4	3	3	22
Broadleaf mixed forest	10	4	2	2	1	19
Pinus yunnanensis	5	11	4	7	1	28
Quercus spp.	7	2	3	2	1	15
Pinus densata	0	2	2	1	5	10
Coniferous forest	0	1	1	2	2	6
Abies spp.	0	0	0	1	3	4
Abies georgei	1	0	1	0	2	4
Abies forrestii	0	0	0	0	3	3
Picea likiangensis	0	0	0	2	1	3
Picea spp.	0	0	0	0	2	2
Alnus nepalensis	2	0	0	1	0	3
Other hard broadleaf species	0	0	0	0	1	1
Other soft broadleaf species	0	0	0	0	1	1
Albizia spp.	0	0	0	0	1	1
Abies spp. (Nujiang fir)	0	0	0	0	1	1
Quercus aquifolioides	1	0	0	0	0	1
Cyclobalanopsis spp.	1	0	0	0	0	1
Cyclobalanopsis myrsinifolia	0	1	0	0	0	1
Juglans regia	0	1	0	0	0	1
Total	32	29	17	21	28	127

References

1. Hall, R.; Skakun, R.; Arsenault, E.; Case, B. Modeling forest stand structure attributes using Landsat ETM+ data: Application to mapping of aboveground biomass and stand volume. *For. Ecol. Manag.* **2006**, *225*, 378–390. https://doi.org/10.1016/j.foreco.2006.01.014.
2. Toaza, J.M.M. Low-Cost and Mobile Lidar Technologies for Forest Inventory: A Review on Accuracy, Efficiency, and Multi-Temporal Monitoring Potential. *Bull. Transilv. Univ. Brasov. Ser. II For. Wood Ind. Agric. Food Eng.* **2026**, *19*, 31–56. https://doi.org/10.31926/but.fwiafe.2026.19.68.1.3.
3. Ullah, S.; Nazeer, M.; Wong, M.S.; Amin, G. Remote sensing for aboveground biomass monitoring in terrestrial ecosystems: A systematic review. *Remote Sens. Appl. Soc. Environ.* **2025**, *39*, 101635. https://doi.org/10.1016/j.rsase.2025.101635.
4. Muhe, S.; Argaw, M. Estimation of above-ground biomass in tropical afro-montane forest using Sentinel-2 derived indices. *Environ. Syst. Res.* **2022**, *11*, 5. https://doi.org/10.1186/s40068-022-00250-y.
5. Huy, B.; Truong, N.Q.; Khiem, N.Q.; Poudel, K.P.; Temesgen, H. Deep learning models for improved reliability of tree above-ground biomass prediction in the tropical evergreen broadleaf forests. *For. Ecol. Manag.* **2022**, *508*, 120031. https://doi.org/10.1016/j.foreco.2022.120031.
6. He, C.; Li, Y.; Dai, X.; Liu, N.; Wu, F.; Yan, J.; Gao, M.; Liang, Y.; Yuan, Z.; Hao, Z. Species richness is not a good predictor for above-ground biomass in a warm temperate deciduous broadleaf forest. *Ecol. Processes* **2025**, *14*, 6. https://doi.org/10.1186/s13717-024-00569-7.
7. Puliti, S.; Saarela, S.; Gobakken, T.; Ståhl, G.; Næsset, E. Combining UAV and Sentinel-2 auxiliary data for forest growing stock volume estimation through hierarchical model-based inference. *Remote Sens. Environ.* **2018**, *204*, 485–497. https://doi.org/10.1016/j.rse.2017.10.007.
8. Mura, M.; Bottalico, F.; Giannetti, F.; Bertani, R.; Giannini, R.; Mancini, M.; Orlandini, S.; Travaglini, D.; Chirici, G. Exploiting the capabilities of the Sentinel-2 multi spectral instrument for predicting growing stock volume in forest ecosystems. *Int. J. Appl. Earth Obs. Geoinf.* **2018**, *66*, 126–134. https://doi.org/10.1016/j.jag.2017.11.013.

9. Chrysafis, I.; Mallinis, G.; Tsakiri, M.; Patias, P. Evaluation of single-date and multi-seasonal spatial and spectral information of Sentinel-2 imagery to assess growing stock volume of a Mediterranean forest. *Int. J. Appl. Earth Obs. Geoinf.* **2019**, *77*, 1–14. https://doi.org/10.1016/j.jag.2018.12.004.
10. Li, X.; Long, J.; Zhang, M.; Liu, Z.; Lin, H. Coniferous plantations growing stock volume estimation using advanced remote sensing algorithms and various fused data. *Remote Sens.* **2021**, *13*, 3468. https://doi.org/10.3390/rs13173468.
11. Liu, P.; Ren, C.; Yang, X.; Wang, Z.; Jia, M.; Zhao, C.; Yu, W.; Ren, H. Combining Sentinel-2 and diverse environmental data largely improved aboveground biomass estimation in China's boreal forests. *Sci. Rep.* **2024**, *14*, 27528. https://doi.org/10.1038/s41598-024-78615-9.
12. Ge, S.; Tomppo, E.; Rauste, Y.; McRoberts, R.E.; Praks, J.; Gu, H.; Su, W.; Antropov, O. Sentinel-1 time series for predicting growing stock volume of boreal forest: Multitemporal analysis and feature selection. *Remote Sens.* **2023**, *15*, 3489. https://doi.org/10.3390/rs15143489.
13. Irannejad, S.; Bagheri, H. Explaining ecological drivers and management implications of forest biomass: An explainable deep learning fusion of remote sensing and climate data. *Trees For. People* **2026**, *24*, 101154. https://doi.org/10.1016/j.tfp.2026.101154.
14. Bountos, N.I.; Ouaknine, A.; Papoutsis, I.; Rolnick, D. Fomo: Multi-modal, multi-scale and multi-task remote sensing foundation models for forest monitoring. *Proc. AAAI Conf. Artif. Intell.* **2025**, *39*, 27858–27868.
15. Cheng, Z.; Gu, X.; Du, Y.; Wei, C.; Xu, Y.; Zhou, Z.; Li, W.; Cai, W. Multi-modal fusion and multi-task deep learning for monitoring the growth of film-mulched winter wheat. *Precis. Agric.* **2024**, *25*, 1933–1957. https://doi.org/10.1007/s11119-024-10147-8.
16. Ma, X.; Wu, Y.; Lin, Z.; Lin, T. TomPhenoNet: A multi-modal fusion and multi-task learning network model for monitoring growth parameters of dwarf tomatoes. *Comput. Electron. Agric.* **2025**, *235*, 110387. https://doi.org/10.1016/j.compag.2025.110387.
17. Niu, Z.; Zhong, G.; Yu, H. A review on the attention mechanism of deep learning. *Neurocomputing* **2021**, *452*, 48–62. https://doi.org/10.1016/j.neucom.2021.03.091.
18. Dong, W.; Mitchard, E.T.; Yu, H.; Hancock, S.; Ryan, C.M. Forest aboveground biomass estimation using GEDI and earth observation data through attention-based deep learning. *arXiv* **2023**, arXiv:2311.03067. https://doi.org/10.48550/arXiv.2311.03067.
19. Wang, B.; Chen, Y.; Yan, Z.; Liu, W. Integrating remote sensing data and CNN-LSTM-Attention Techniques for improved forest stock volume Estimation: A Comprehensive analysis of Baishanzu Forest Park, China. *Remote Sens.* **2024**, *16*, 324. https://doi.org/10.3390/rs16020324.
20. Elharrouss, O.; Mahmood, Y.; Bechqito, Y.; Serhani, M.A.; Badidi, E.; Riffi, J.; Tairi, H. Task-based loss functions in computer vision: A comprehensive review. *arXiv* **2025**, arXiv:2504.04242. https://doi.org/10.48550/arXiv.2504.04242.
21. Yu, T.; Kumar, S.; Gupta, A.; Levine, S.; Hausman, K.; Finn, C. Gradient surgery for multi-task learning. *Adv. Neural Inf. Process. Syst.* **2020**, *33*, 5824–5836. https://doi.org/10.48550/arXiv.2001.06782.
22. Kirchdorfer, L.; Sesterhenn, T.; Bartelt, C.; Stuckenschmidt, H.; Schott, L.; Köhler, J.M. Investigating Uncertainty Weighting for Multi-Task Learning: Insights and Analytical Alternative. *Int. J. Comput. Vis.* **2026**, *134*, 8. https://doi.org/10.1007/s11263-025-02625-x.
23. Xu, Q.; Lei, X.; Zhang, H. A novel method for approaching the compatibility of tree biomass estimation by multi-task neural networks. *For. Ecol. Manag.* **2022**, *508*, 120011. https://doi.org/10.1016/j.foreco.2022.120011.
24. Qin, J.; Ma, M.; Zhu, Y.; Wu, B.; Su, X. 3PG-MT-LSTM: A hybrid model under biomass compatibility constraints for the prediction of long-term forest growth to support sustainable management. *Forests* **2023**, *14*, 1482. https://doi.org/10.3390/f14071482.
25. Xie, S.; Yan, T.; Sun, X.; Chen, H.; Sun, M.; Zhang, Y. Radial growth response of Pinus Yunnanensis to climate in high mountain forests of northwestern Yunnan, southwestern China. *Front. For. Glob. Change* **2024**, *7*, 1343730. https://doi.org/10.3389/ffgc.2024.1343730.
26. Yan, W.; He, Y.; Cai, Y.; Qu, X.; Cui, X. Relationship between extreme climate indices and spatiotemporal changes of vegetation on Yunnan Plateau from 1982 to 2019. *Glob. Ecol. Conserv.* **2021**, *31*, e01813. https://doi.org/10.1016/j.gecco.2021.e01813.
27. Huo, H.; Sun, C. Spatiotemporal variation and influencing factors of vegetation dynamics based on Geodetector: A case study of the northwestern Yunnan Plateau, China. *Ecol. Indic.* **2021**, *130*, 108005. https://doi.org/10.1016/j.ecolind.2021.108005.
28. Cheng, W.C.; Fu, L.K. *Flora Reipublicae Popularis Sinicae*; Science Press: Beijing, China, 1978; Volume 7.
29. POWO. Plants of the World Online. Available online: https://powo.science.kew.org/taxon/urn:lsid:ipni.org:names:677024-1 (accessed on 6 September 2026).
30. Wu, Z.-Y.; Raven, P.H. *Flora of China*; Science Press; Missouri Botanical Garden Press: St. Louis, MO, USA, 1999; Volume 4.
31. Song, Y.-C.; Wang, X.-H.; Yan, E.-R. *Evergreen Broad-Leaved Forests in China: Classification, Ecology, Conservation*; Science Press: Beijing, China, 2013.
32. Kim, E.; Lee, W.-K.; Yoon, M.; Lee, J.-Y.; Son, Y.; Abu Salim, K. Estimation of voxel-based above-ground biomass using airborne LiDAR data in an intact tropical rain forest, Brunei. *Forests* **2016**, *7*, 259. https://doi.org/10.3390/f7110259.

33. *GB/T 26424-2010*; Technical Regulations for Inventory for Forest Management Planning and Design; China Standards Press: Beijing, China, 2010.
34. State Forestry Administration of China. *Technical Regulation for Tree Biomass Modeling*; Standards Press of China: Beijing, China, 2014.
35. Ghosh, S.M.; Behera, M.D. Aboveground biomass estimation using multi-sensor data synergy and machine learning algorithms in a dense tropical forest. *Appl. Geogr.* **2018**, *96*, 29–40. https://doi.org/10.1016/j.apgeog.2018.05.011.
36. Ye, Q.; Yu, S.; Liu, J.; Zhao, Q.; Zhao, Z. Aboveground biomass estimation of black locust planted forests with aspect variable using machine learning regression algorithms. *Ecol. Indic.* **2021**, *129*, 107948. https://doi.org/10.1016/j.ecolind.2021.107948.
37. Belgiu, M.; Drăguţ, L. Random forest in remote sensing: A review of applications and future directions. *ISPRS J. Photogramm. Remote Sens.* **2016**, *114*, 24–31. https://doi.org/10.1016/j.isprsjprs.2016.01.011.
38. Zhao, Y.; Guo, F.; Wang, Y.; Huang, J.; Peng, D. Estimating forest growing stock volume using feature selection and advanced remote sensing algorithm. *Remote Sens. Appl. Soc. Environ.* **2025**, *37*, 101458. https://doi.org/10.1016/j.rsase.2025.101458.
39. Fang, J.-Y.; Wang, G.G.; Liu, G.-H.; Xu, S.-L. Forest biomass of China: An estimate based on the biomass–volume relationship. *Ecol. Appl.* **1998**, *8*, 1084–1091. https://doi.org/10.1890/1051-0761(1998)008[1084:FBOCAE]2.0.CO;2.
40. Brown, S.; Lugo, A.E. Biomass of tropical forests: A new estimate based on forest volumes. *Science* **1984**, *223*, 1290–1293. https://doi.org/10.1126/science.223.4642.1290.
41. Breiman, L. Random forests. *Mach. Learn.* **2001**, *45*, 5–32. https://doi.org/10.1023/A:1010933404324.
42. Chen, T.; Guestrin, C. Xgboost: A scalable tree boosting system. In Proceedings of the 22nd ACM SIGKDD international conference on knowledge discovery and data mining, San Francisco, CA, USA, 13–17 August 2016; pp. 785–794.
43. Cover, T.; Hart, P. Nearest neighbor pattern classification. *IEEE Trans. Inf. Theory* **1967**, *13*, 21–27. https://doi.org/10.1109/TIT.1967.1053964.
44. Dorogush, A.V.; Ershov, V.; Gulin, A. CatBoost: Gradient boosting with categorical features support. *arXiv* **2018**, arXiv:1810.11363. https://doi.org/10.48550/arXiv.1810.11363.
45. Suleymanov, A.; Bogdan, E.; Gaysin, I.; Volkov, A.; Tuktarova, I.; Belan, L.; Shagaliev, R. Spatial high-resolution modelling and uncertainty assessment of forest growing stock volume based on remote sensing and environmental covariates. *For. Ecol. Manag.* **2024**, *554*, 121676. https://doi.org/10.1016/j.foreco.2023.121676.
46. Cheng, Z.; Aakala, T.; Larjavaara, M. Elevation, aspect, and slope influence woody vegetation structure and composition but not species richness in a human-influenced landscape in northwestern Yunnan, China. *Front. For. Glob. Change* **2023**, *6*, 1187724. https://doi.org/10.3389/ffgc.2023.1187724.
47. Anees, S.A.; Mehmood, K.; Khan, W.R.; Sajjad, M.; Alahmadi, T.A.; Alharbi, S.A.; Luo, M. Integration of machine learning and remote sensing for above ground biomass estimation through Landsat-9 and field data in temperate forests of the Himalayan region. *Ecol. Inform.* **2024**, *82*, 102732. https://doi.org/10.1016/j.ecoinf.2024.102732.
48. Paré, D.; Bognounou, F.; Emilson, E.J.; Laganière, J.; Leach, J.; Mansuy, N.; Martineau, C.; Norris, C.; Venier, L.; Webster, K. Connecting forest soil properties with ecosystem services: Toward a better use of digital soil maps—A review. *Soil Sci. Soc. Am. J.* **2024**, *88*, 981–999. https://doi.org/10.1002/saj2.20705.
49. Zhang, Y.; Liu, J.; Li, W.; Liang, S. A proposed ensemble feature selection method for estimating forest aboveground biomass from multiple satellite data. *Remote Sens.* **2023**, *15*, 1096. https://doi.org/10.3390/rs15041096.
50. Phillips, O.L.; Sullivan, M.J.; Baker, T.R.; Monteagudo Mendoza, A.; Vargas, P.N.; Vásquez, R. Species matter: Wood density influences tropical forest biomass at multiple scales. *Surv. Geophys.* **2019**, *40*, 913–935. https://doi.org/10.1007/s10712-019-09540-0.
51. Xu, Q.; Li, B.; McRoberts, R.E.; Li, Z.; Hou, Z. Harnessing data assimilation and spatial autocorrelation for forest inventory. *Remote Sens. Environ.* **2023**, *288*, 113488. https://doi.org/10.1016/j.rse.2023.113488.
52. Willmott, C.J.; Matsuura, K. Advantages of the mean absolute error (MAE) over the root mean square error (RMSE) in assessing average model performance. *Clim. Res.* **2005**, *30*, 79–82. https://doi.org/10.3354/cr030079.
53. Emick, E.; Babcock, C.; White, G.W.; Hudak, A.T.; Domke, G.M.; Finley, A.O. An approach to estimating forest biomass while quantifying estimate uncertainty and correcting bias in machine learning maps. *Remote Sens. Environ.* **2023**, *295*, 113678. https://doi.org/10.1016/j.rse.2023.113678.
54. Coops, N.C.; Tompalski, P.; Goodbody, T.R.; Queinnec, M.; Luther, J.E.; Bolton, D.K.; White, J.C.; Wulder, M.A.; van Lier, O.R.; Hermosilla, T. Modelling lidar-derived estimates of forest attributes over space and time: A review of approaches and future trends. *Remote Sens. Environ.* **2021**, *260*, 112477. https://doi.org/10.1016/j.rse.2021.112477.
55. Xu, X.; Lin, H.; Liu, Z.; Ye, Z.; Li, X.; Long, J. A combined strategy of improved variable selection and ensemble algorithm to map the growing stem volume of planted coniferous forest. *Remote Sens.* **2021**, *13*, 4631. https://doi.org/10.3390/rs13224631.

56. Francini, S.; Borghi, C.; D'Amico, G.; Waser, L.T.; Lisiewicz, M.; Stereńczak, K.; Schelhaas, M.-J.; Pellett, C.; Gobakken, T.; Næsset, E. Bridging spatio-temporal gaps in ALS data using Landsat time series and forest disturbance-recovery metrics via multi-task neural networks. *Sci. Remote Sens.* **2025**, *12*, 100318. https://doi.org/10.1016/j.srs.2025.100318.
57. Xiang, B.; Wielgosz, M.; Kontogianni, T.; Peters, T.; Puliti, S.; Astrup, R.; Schindler, K. Automated forest inventory: Analysis of high-density airborne LiDAR point clouds with 3D deep learning. *Remote Sens. Environ.* **2024**, *305*, 114078. https://doi.org/10.1016/j.rse.2024.114078.
58. Wang, T.; Dong, L.; Liu, Z. Factors driving carbon accumulation in forest biomass and soil organic carbon across natural forests and planted forests in China. *Front. For. Glob. Change* **2024**, *6*, 1333868. https://doi.org/10.3389/ffgc.2023.1333868.
59. Uyar, N. Tropical forest biomass assessment using LIDAR, DEM, and Sentinel-2 in the Daintree forest. *Plant Ecol.* **2026**, *227*, 42. https://doi.org/10.1007/s11258-026-01602-9.
60. Nava-Nava, A.; Santiago-García, W.; Quiñonez-Barraza, G.; Santos-Posadas, H.M.d.L.; Valdez-Lazalde, J.R.; Ángeles-Pérez, G. Climatic and topographic variables improve estimation accuracy of Patula pine forest site productivity in Southern Mexico. *Forests* **2022**, *13*, 1277. https://doi.org/10.3390/f13081277.
61. Tompalski, P.; White, J.C.; Coops, N.C.; Wulder, M.A. Demonstrating the transferability of forest inventory attribute models derived using airborne laser scanning data. *Remote Sens. Environ.* **2019**, *227*, 110–124. https://doi.org/10.1016/j.rse.2019.04.006.
62. Wang, G.; Dong, W.; Zhang, H.; Ji, Y.; Zhang, W.; Zhao, H.; Wang, M.; Ma, Y.; Song, C.; Jiang, Y. Transferability of aboveground biomass estimation using Sentinel-1/2 and GEDI data in subtropical forests of complex terrain, China. *iScience* **2026**, *29*, 115346. https://doi.org/10.1016/j.isci.2026.115346.
63. He, Y.; Shu, S.; Holm, J.; Needham, J.; Negron-Juarez, R.; Koven, C.; Zhu, Q.; Falco, N. Forest aboveground biomass estimation through integration of sentinel-2 and PALSAR-2 time series: Assessing models trained on GEDI and field inventory benchmarks. *ISPRS J. Photogramm. Remote Sens.* **2026**, *236*, 668–689. https://doi.org/10.1016/j.isprsjprs.2026.04.022.

Disclaimer/Publisher's Note: The statements, opinions and data contained in all publications are solely those of the individual author(s) and contributor(s) and not of MDPI and/or the editor(s). MDPI and/or the editor(s) disclaim responsibility for any injury to people or property resulting from any ideas, methods, instructions or products referred to in the content.